Supplementary Information (SI) for Journal of Materials Chemistry A.

Boosting Surface Reconstruction in Engineered Nickel Sites through Selenium Vacancies to Enhance Urea Oxidation Reaction

Fakhr uz Zaman [a, b] Azhar Saeed [a, b], Fekadu Tsegaye Dajan [a, d], Usman Ghani [a, f], Amir Said [e], Muhammad Ahmad [a, f], Shemsu Ligani [a, f], Khan Abdul Sammed [a, b], Sikandar Iqbal [c] *, Felix Ofori Boakye [a, b] *

[a] Institute for Advanced Study, Shenzhen University, Shenzhen 518060, China.

[b] College of Physics and Optoelectronic Engineering, Shenzhen University, Shenzhen 518060, China.

[c] Institute of Energy Materials Science University of Shanghai for Science and Technology, Shanghai 200093, China

[d] College of Civil and Transportation Engineering Shenzhen University, Guangdong 518060, China.

[e] Center of Information Photonics and Energy Materials, Shenzhen Institute of Advance Technology, Chinese Academy of Sciences, Shenzhen 518055, China

[f] College of Civil and Transportation Engineering Shenzhen University Guangdong 518060, China

Corresponding authors:

sikandar@zju.edu.cn (S. Iqbal)

felix88@whut.edu.cn (F.O. Boakye)

1.1. Electrochemical active surface area (ECSA) calculation

The electrochemically active surface area (ECSA) of the prepared materials were analyzed by calculating the double-layer capacitance (C_{dl}), which was derived from cyclic voltammetry (CV) plots in the non-Faradaic area, from 0.1 to 0.2 V (vs. Hg/HgO), at (10 - 50 mV s^{-1}) scan rates. The capacitive current densities, obtained by averaging the slopes of both the anodic and cathodic segments of the linear fit, were used for these measurements. The slope of the linear fit provided the C_{dl} value, and the specific capacitance was determined to be 60 μFcm^{-2}. also, the ECSA of the catalysts in their current state can be determined using the equation $ECSA = \frac{C_{dl}}{C_s}$.

1.2. Turnover frequency (TOF) calculations

The turnover frequency (TOF) measurements for various catalysts were conducted. TOF, which represents the reaction rate per active site, is utilized to compare the intrinsic activity of different prepared materials. The TOF value was analyzed from the equation below;

$$\text{TOF} = \frac{JA}{4FN_s}$$

J represents the current density at the specified overpotential, A denotes the material surface area, F is the Faraday constant (96485 C mol^{-1}), and Ns signifies the number of active sites per sample. For the redox reaction in 1.0 M KOH + 0.5 M urea, the value of Ns was determined using cyclic voltammetry (CV) curves at different scan rates. The slope was derived from the plot of peak current versus scan rate as described below.

$$\text{slope} = \frac{n^2xF^2AxN_s}{4RT}$$

Here, n represents the number of electrons transferred (n = 1), F refers to the Faraday constant, A indicates the surface area of the sample, Ns stands for the surface concentration of active sites, while R and T are the gas constant and temperature, respectively.

1.3. In situ IRRAS Spectroscopy

In this study, an A-type mercuric cadmium telluride (MCT) detector was used in conjunction with a Nicolet iS50 spectrometer to perform in-situ infrared reflection-absorption spectroscopy (IRRAS). The working electrode, a Se_{vac}@NiSe-NS catalyst, was positioned on the Si face-angle within an electrochemical three-electrode cell. This setup included a platinum wire as the counter electrode and an Ag/AgCl electrode as the reference electrode. The urea oxidation reaction (UOR) experiments were carried out using 1 M KOH + 0.5 M urea. The working electrode was placed against the flat surface of a ZnSe hemisphere for the measurements.

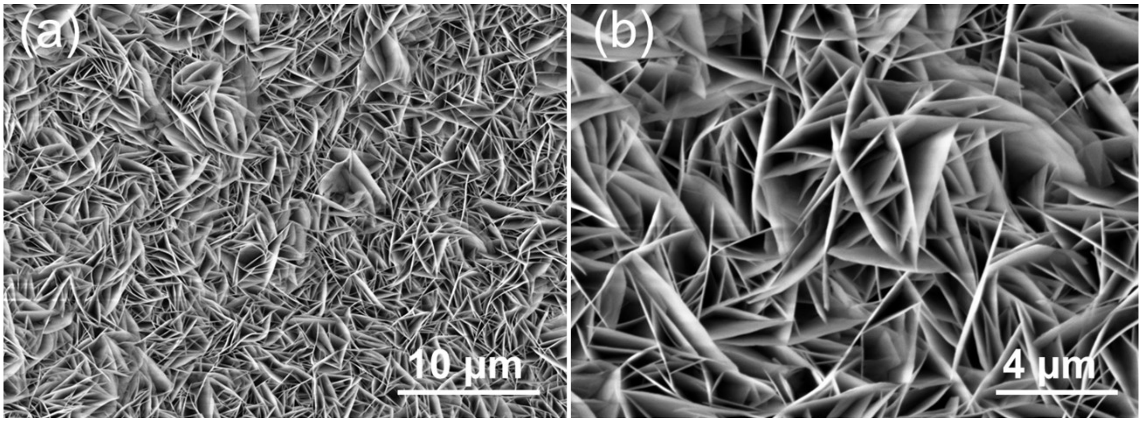

Fig. S1. (a, b) SEM images of $Ni(OH)_2$

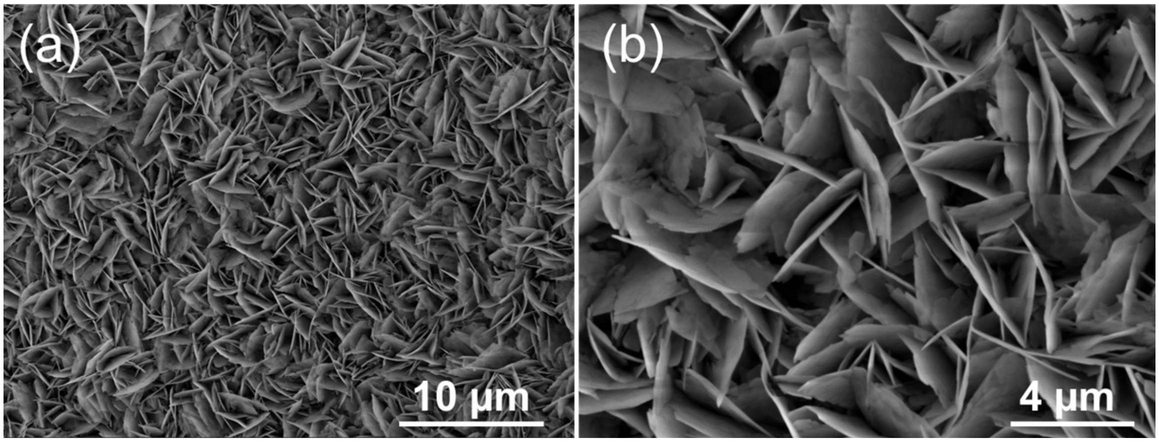

Fig. S2. (a, b) SEM images of NiSe

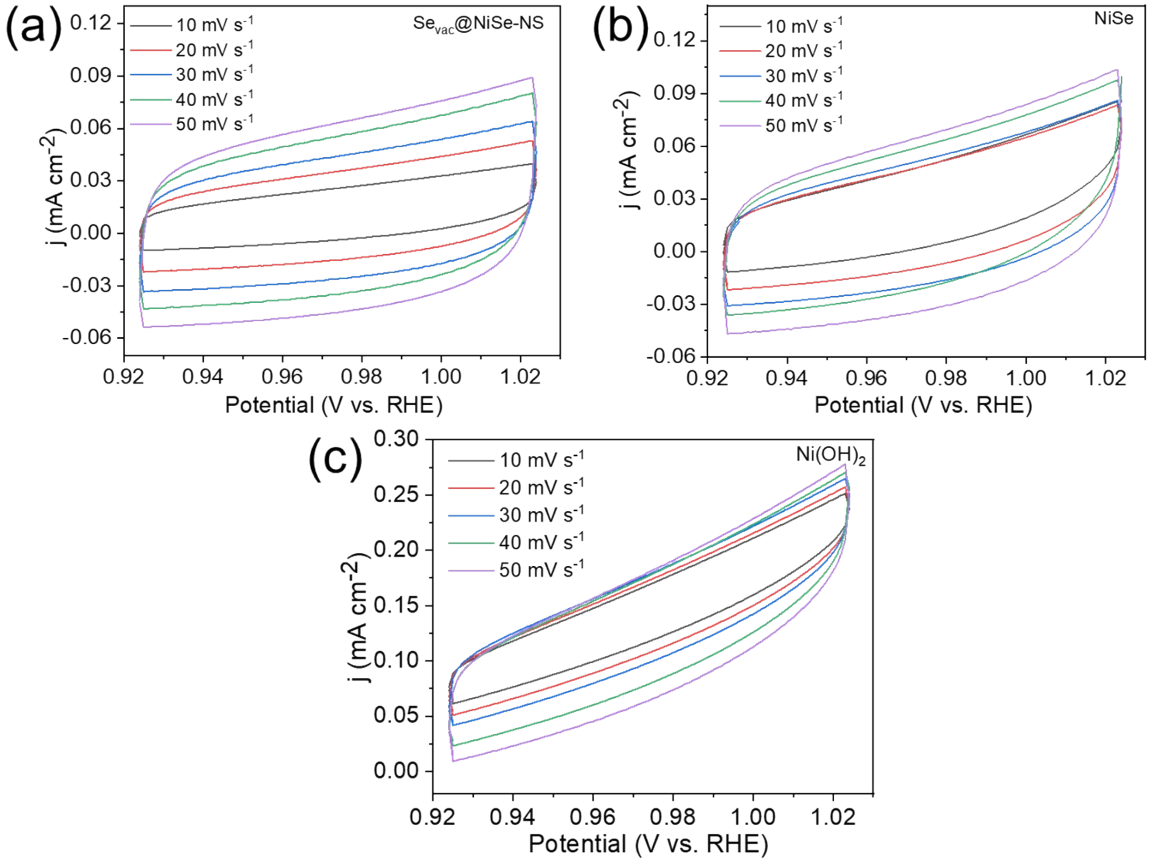

Fig. S3. (a,b,c) CV curves of Se$_{vac}$@NiSe-NS, NiSe and Ni(OH)$_2$ recorded at different scan rates for UOR.

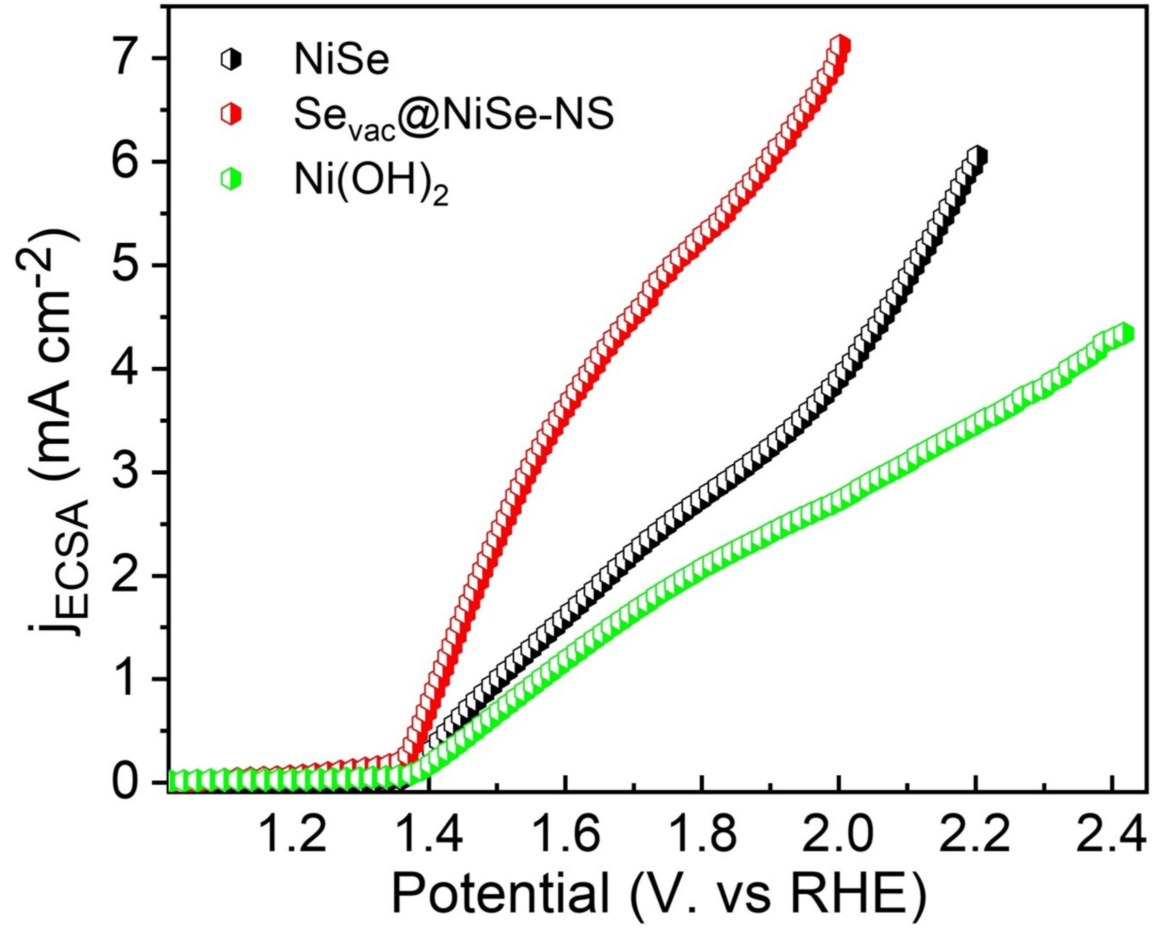

Fig. S4. Polarization curves normalized by electrochemical active surface area.

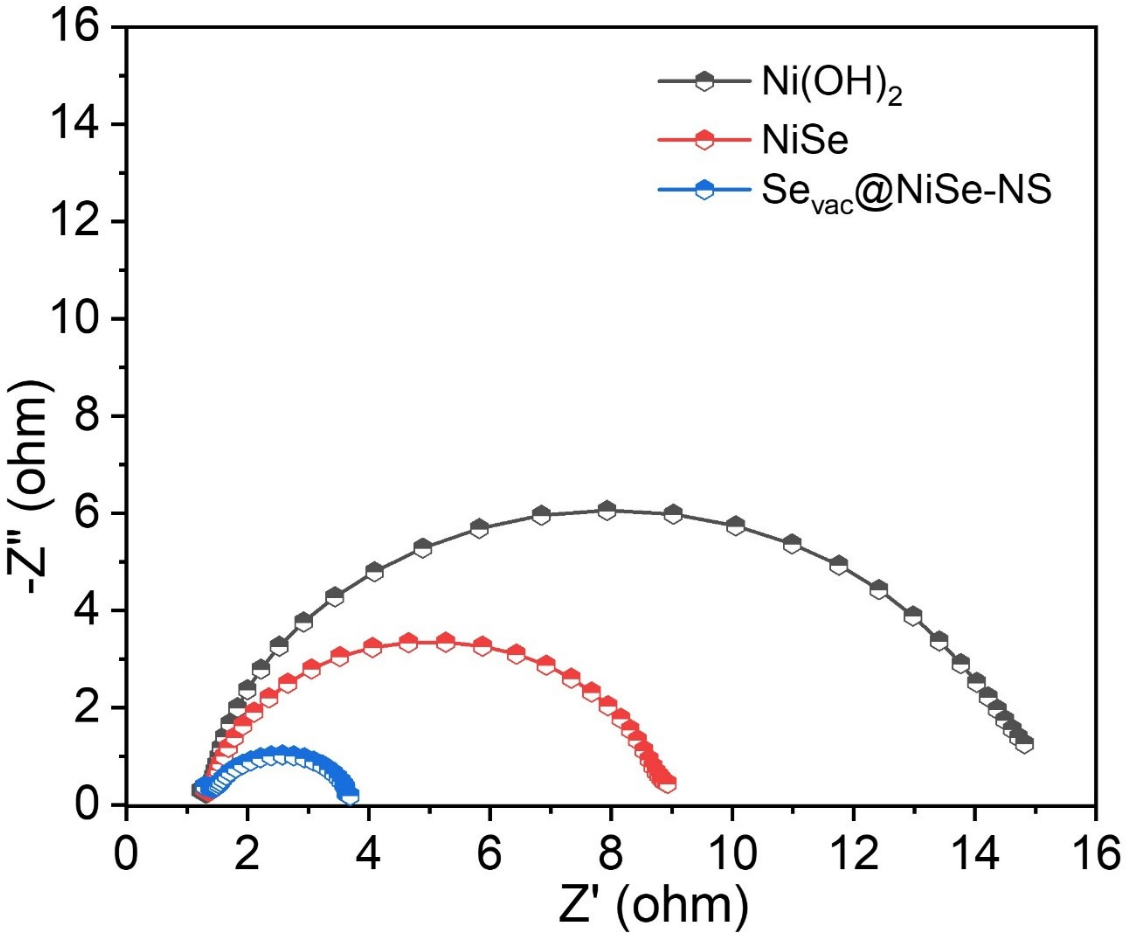

Fig. S5. Nyquist plots for Ni (OH)$_2$, NiSe and Se$_{vac}$@NiSe-NS

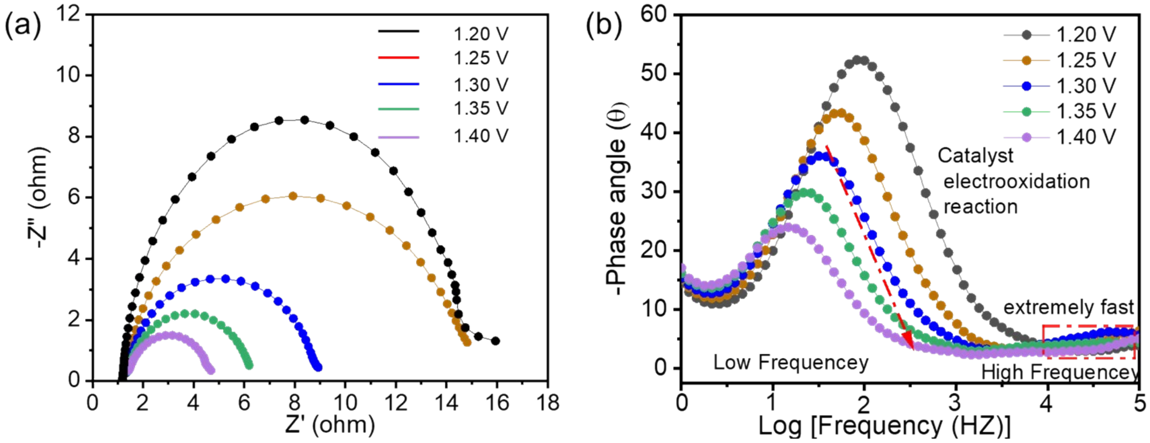

Figure. S6a Nyquist plots at different potential (S6b) Bode plots were recorded at various potentials (versus RHE) for Se_{Vac}@NiSe-NS during the UOR.

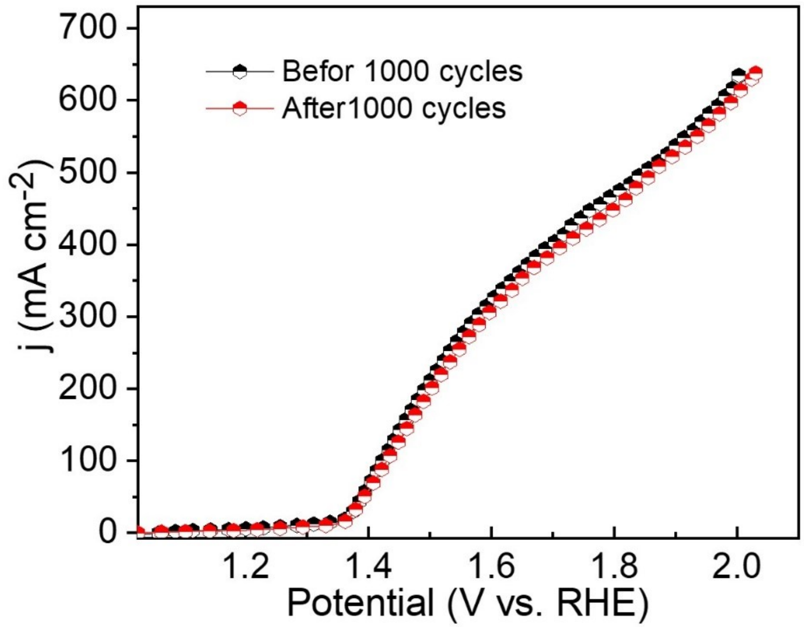

Fig. S7. LSV curve of Se$_{vac}$@NiSe-NS after 1000 CV cycles.

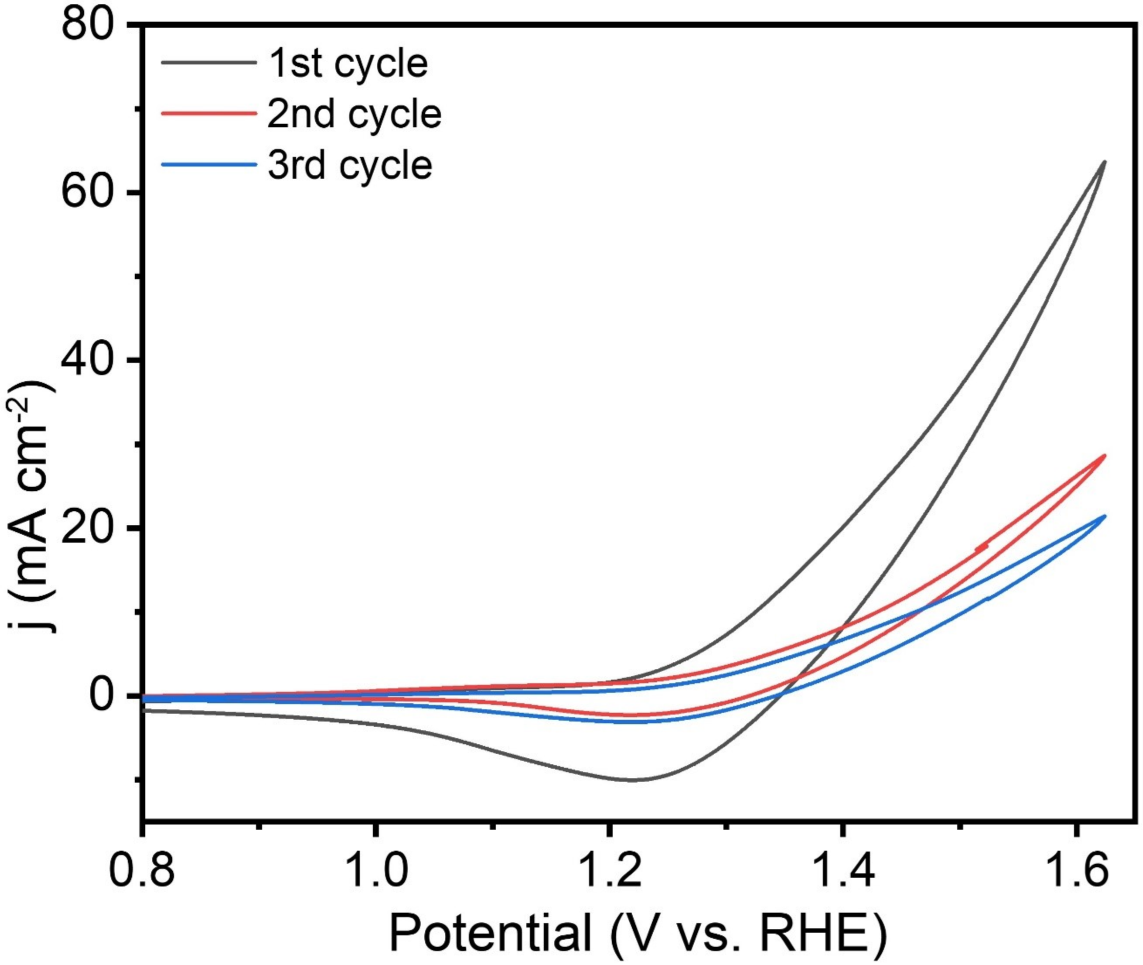

Fig. S8. CV scan for Se$_{vac}$@NiSe-NS showing its electrochemical reconstruction.

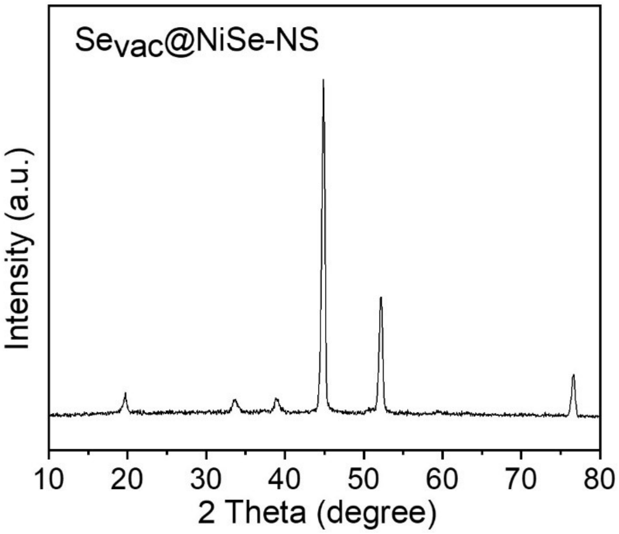

Fig. S9. XRD pattern of Se$_{vac}$@NiSe-NS after UOR reaction

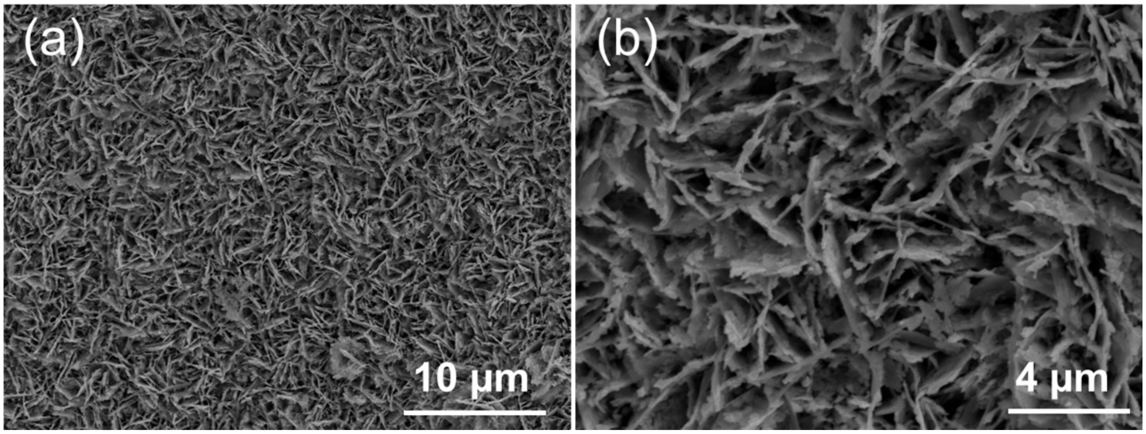

Fig. S10. (a, b) SEM images of Se_{vac}@NiSe-NS after UOR reaction.

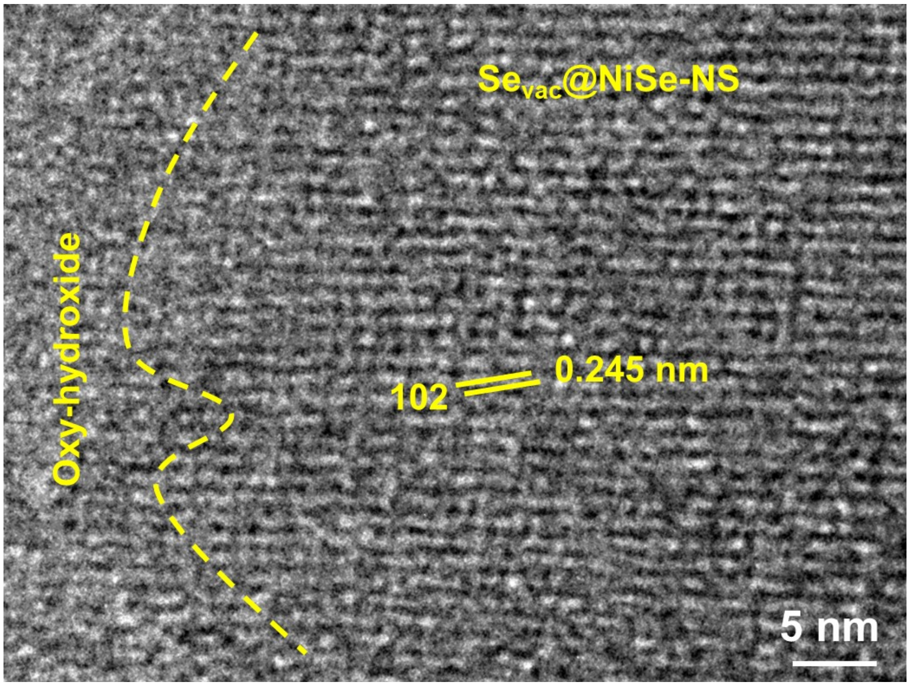

Fig. S11. HRTEM image of Se$_{vac}$@NiSe-NS after stability

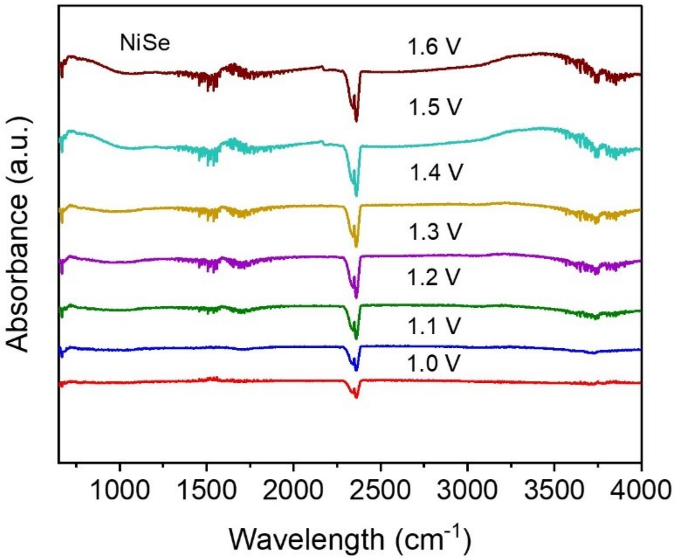

Fig. S12. Insitu-IRRAS spectra of NiSe.

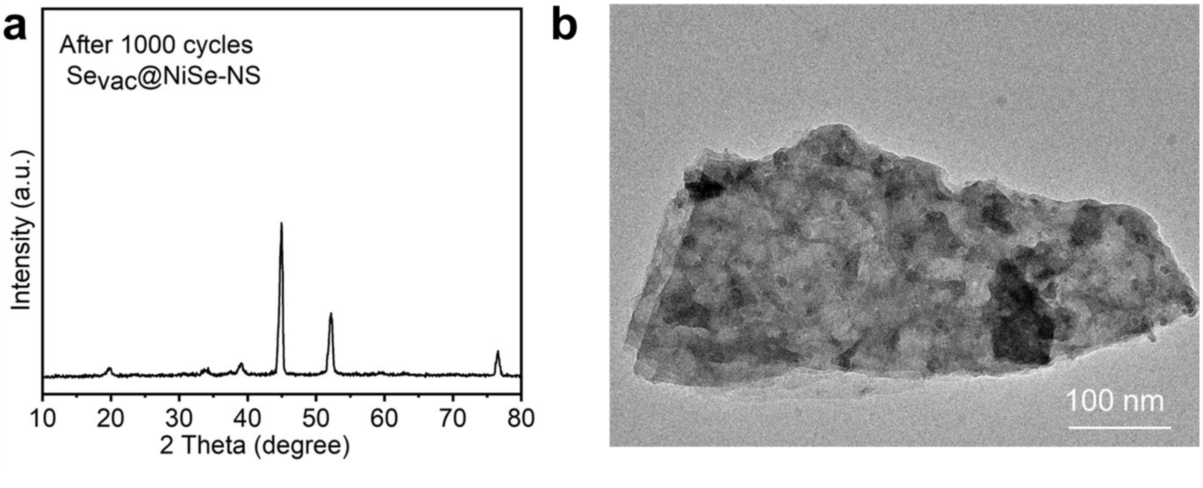

Fig. S13. (a and b) XRD and TEM after 1000 cycles.

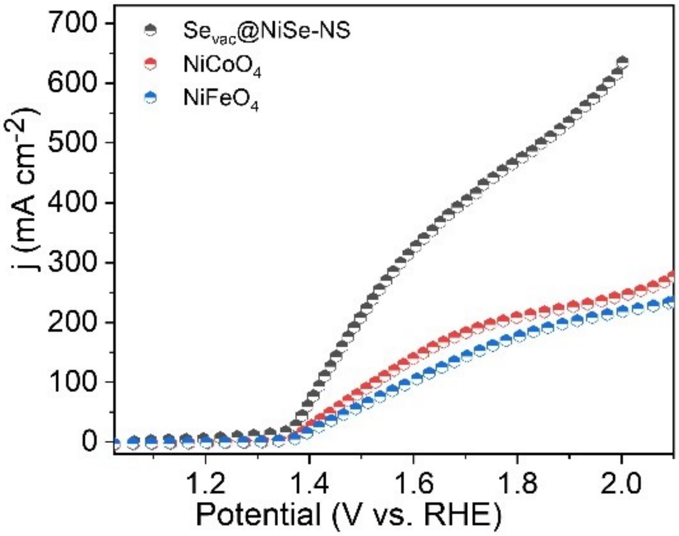

Fig. S14 UOR performance of $NiCo_2O_4$, $NiFe_2O_4$ and Se$_{vac}$@NiSe-NS.

We have conducted a comparative study of $NiCo_2O_4$ and $NiFe_2O_4$ with Se$_{vac}$@NiSe-NS. The results clearly demonstrate that Se$_{vac}$@NiSe-NS exhibits significantly enhanced performance over the other samples. The superior activity can be attributed to the intrinsic properties of Se-based materials, which were strategically selected for the UOR reaction due to their unique electronic structure and excellent electrical conductivity. Unlike Fe and Co, Se features a higher metallic character and lower electronegativity, leading to improved intrinsic conductivity and a narrower bandgap. These advantages greatly enhance charge transfer efficiency and accelerate reaction kinetics, ultimately boosting the overall catalytic performance.

Scalability Testing of Se_{vac}@NiSe-NS for UOR

To assess the scalability, the performance of the large-scale synthesized Se_{vac}@NiSe-NS catalyst was evaluated under same electrochemical testing conditions as the small-scale. As shown in **Fig.** S15, the electrocatalytic activity for UOR remained almost the same despite the increased synthesis scale, indicating excellent reproducibility and consistency.

The catalyst exhibited comparable overpotentials and current densities suggesting that the active sites remained effective even after upscaling. Also, the catalyst layer stayed well attached to the nickel foam and didn't show any peeling or cracks.

These results confirm the robustness of our synthesis protocol for scale-up applications. The ability to retain catalytic performance at higher loadings demonstrates the potential of Se_{vac}@NiSe-NS for practical deployment in industrial-scale UOR systems.

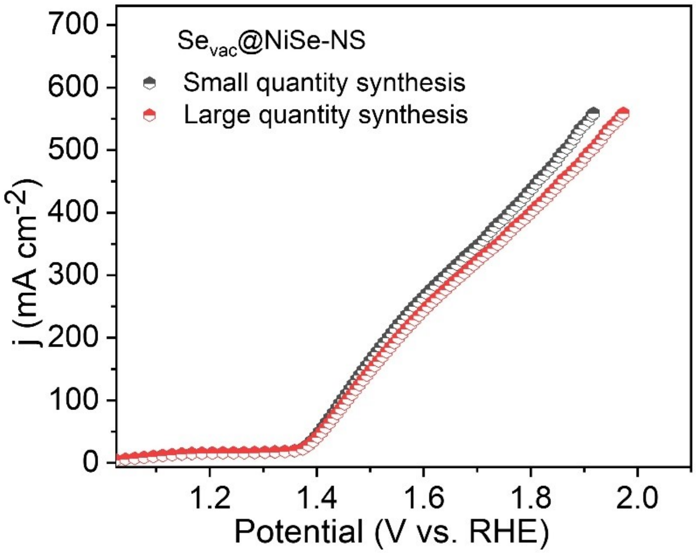

Fig. S15 UOR performance comparison of Se_{vac}@NiSe-NS prepared in small quantity synthesis (black color) and large quantity synthesis (red color) synthesis. LSV curve for small quantity synthesis is taken from Fig.3a.

The lateral size distribution of Se_{vac}@NiSe-NS was evaluated with scanning electron microscopy (SEM) with a nanosheet structure of 191-230 nm lateral size. This relatively narrow size distribution indicates a uniform morphology, which is beneficial for consistent electrochemical behavior. Moreover, such uniformity supports uniform dispersion on the Ni foam substrate, ensuring efficient exposure of active sites and facilitating optimal mass and electron transport, ultimately enhancing the electrode's overall performance.

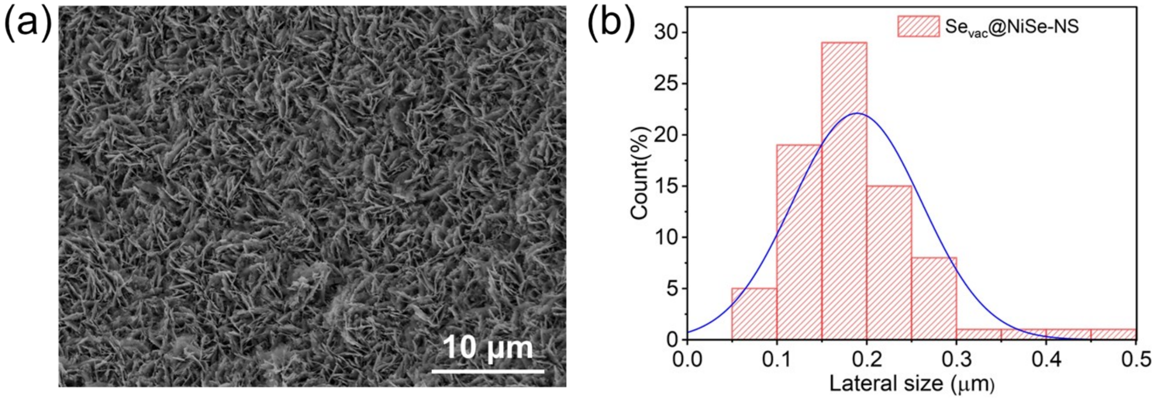

Fig. S16 (a) SEM image of Se_{vac}-NiSe-NS (b) Lateral size distribution histogram of Se_{vac}-NiSe-NS in which the sizes of 80 nanosheets were measured for lateral size distribution analysis.

To gain a comprehensive understanding of its rate capability and versatility, intermediate current densities should also be evaluated. For this purpose, we have tested the material in both 1 M KOH and 1 M KOH + 0.5 M urea. The electrode exhibits excellent stability in 1 M KOH with negligible degradation, while in 1 M KOH + 0.5 M urea, a slight degradation is observed. This enhanced stability in 1 M KOH is attributed to the absence of urea oxidation intermediates that can block active sites. In contrast, during UOR, the formation of by-products such as cyanate and carbonate can lead to partial surface blockage and mild structural degradation. Additionally, the complex multistep nature of UOR introduces higher reaction overpotentials, contributing to performance decline. The stability difference may also come from the competitive adsorption between urea and hydroxide ions, affecting the catalyst's active surface dynamics. Evaluating performance across varying conditions helps identify limitations and ensures broader applicability of the electrode.

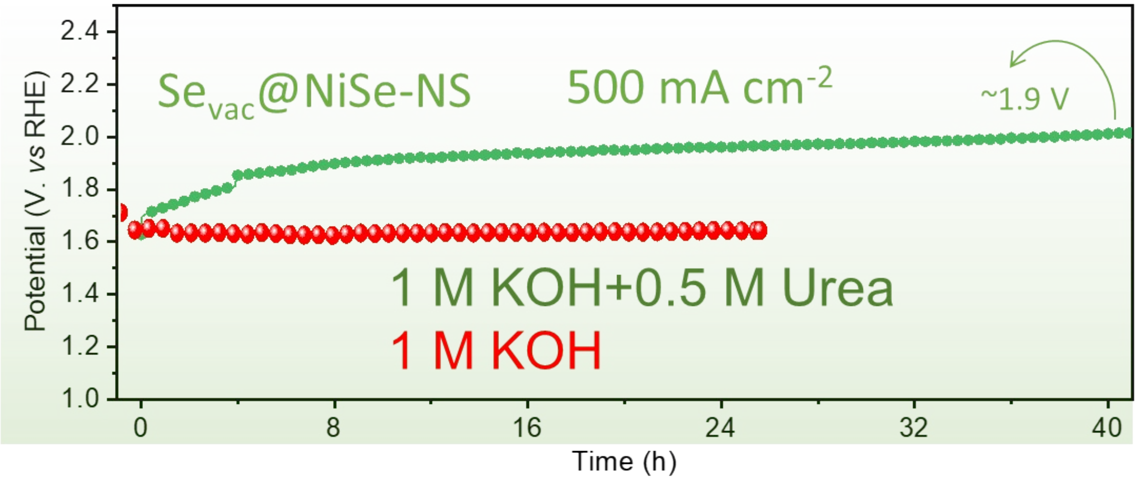

Fig. S17 Chronopotentiometry test of Se$_{vac}$@NiSe-NS at a current density of 500 mA cm^{-2} in 1 M KOH+0.5 M urea and 1 M KOH.

It is possible to control the content of Se vacancies in Se_{vac}@NiSe-NS using sodium borohydride ($NaBH_4$) as a reducing agent. The reaction conditions of $NaBH_4$, particularly the reaction time, can influence the extent of selenium reduction and the formation of Se vacancies. To investigate this effect, we prepared samples with different reduction times Se_{vac}@NiSe-NS-30, Se_{vac}@NiSe-NS-60, and Se_{vac}@NiSe-NS-90, and found that Se_{vac}@NiSe-NS-60 exhibited better performance compared to the others.

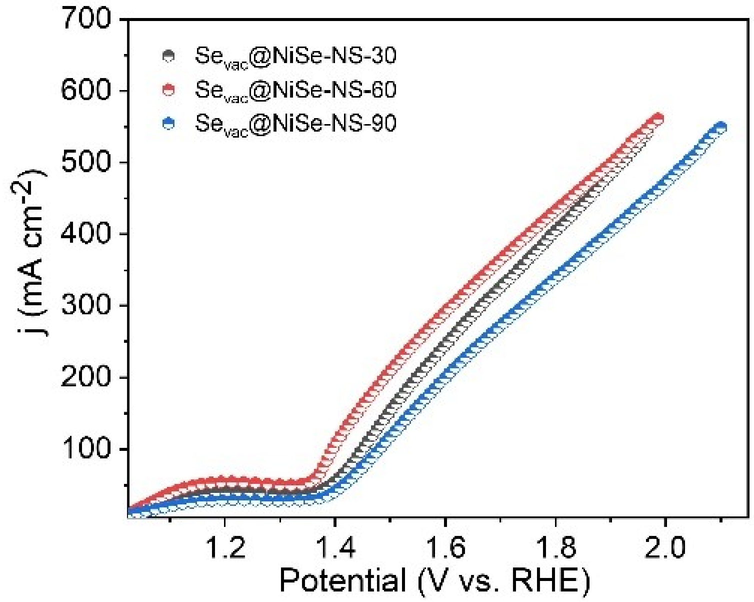

Fig.S18 UOR performance of Se_{vac}@NiSe-NS-30, Se_{vac}@NiSe-NS-60 and Se_{vac}@NiSe-NS-90.

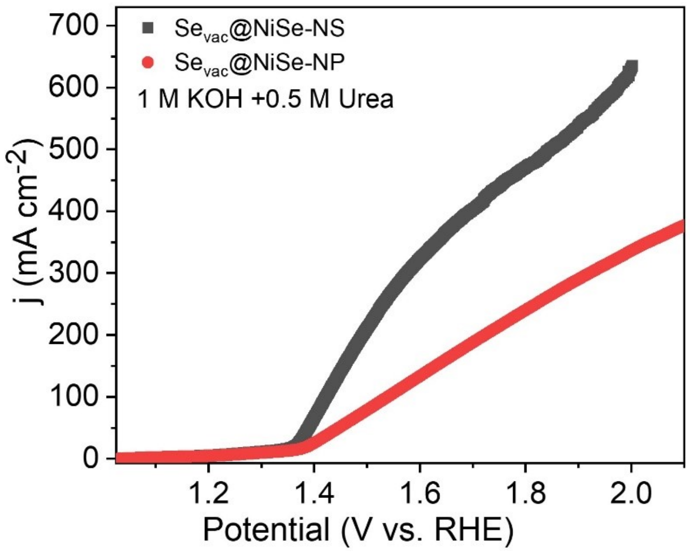

Fig. S19 UOR performance comparison of Se$_{vac}$@NiSe-NS (black color) and (red color) for NiSe-NP. LSV curve for Se$_{vac}$@NiSe-NS is taken from Fig.3 a.

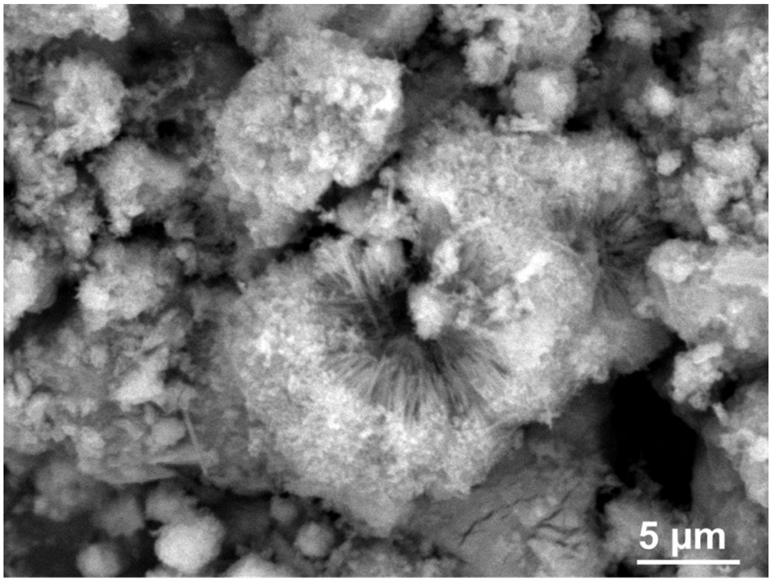

Fig. S20 SEM image of Se_{vac}@NiSe-NP.

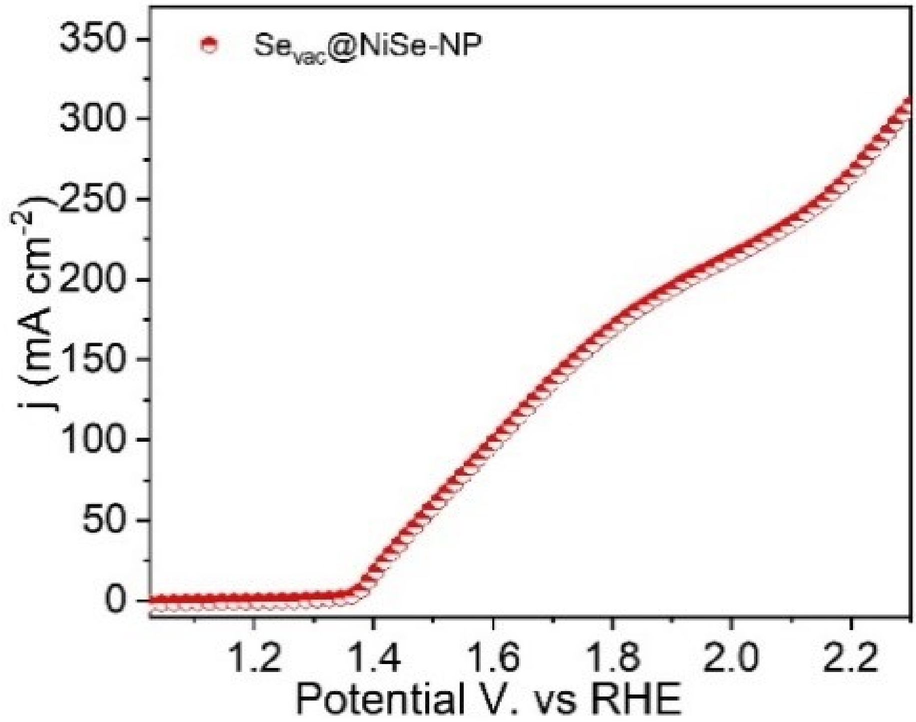

Fig. 21 UOR performance of Se$_{vac}$@NiSe-NP.

Table S1. Performance comparison of different UOR catalysts. All electrochemical activities were obtained from 1 M KOH+ 0.5 M urea.

Catalysts	**Potential @100 (mA cm^{-2}) V vs. RHE**	**Tafel slope (mV dec^{-1})**	**Stability**	**Reference**
Sevac@NiSe-NS/NF	**1.40**	**35.1**	**40 h**	**This work**
Ni-WOx	1.42	39	10 h	[1]
NCVS-3	1.55	37.3	10 h	[2]
O-NiMoP/NF	1.41	36.5	40 h	[3]
Rh/NiV-LDH	1.38	36	36 h	[4]
NC-PB@CNT	1.41	62	30 h	[5]
P-$CoNi_2S_4$	1.55	40	32 h	[6]
$Ni(OH)_2$ (O_{vac}-V-$Ni(OH)_2$)	1.47	29.12	35 h	[7]

Table S2. Cycling Performance comparison of different UOR catalysts. All electrochemical activities were obtained from 1 M KOH+ 0.5 M urea.

Catalysts	**Current density 300**	**Cycles**	**performance**	**Reference**
Se_{vac}@NiSe-NS/NF	**300**	**1000**	**Excellent**	**This work**
Cu_2Se-based	250	500	Poor	[8]
Zn@Ni-MOF	300	800	Good	[9]
$NiSe_2$ nanowrinkles	200	500	poor	[10]
Ni-WOX	200	500	Good	[11]
P-$CoNi_2S_4$	300	700	Good	[12]
Cu0.5Ni0.5/NF	250	500	Good	[13]
CoMn/$CoMn_2O_4$	300	750	Good	[14]
$NiSO_X$	200	500	Poor	[15]
Mo-NiS	200	500	Poor	[16]

References

[1] L. Wang, Y. Zhu, Y. Wen, S. Li, C. Cui, F. Ni, Y. Liu, H. Lin, Y. Li, H. Peng, Angewandte Chemie, 133 (2021) 10671-10676.

[2] Z. Ji, Y. Song, S. Zhao, Y. Li, J. Liu, W. Hu, ACS catalysis, 12 (2021) 569-579.

[3] H. Jiang, M. Sun, S. Wu, B. Huang, C.S. Lee, W. Zhang, Advanced Functional Materials, 31 (2021) 2104951.

[4] H. Sun, L. Li, H.-C. Chen, D. Duan, M. Humayun, Y. Qiu, X. Zhang, X. Ao, Y. Wu, Y. Pang, Science Bulletin, 67 (2022) 1763-1775.

[5] S.A. Patil, S. Cho, Y. Jo, N.K. Shrestha, H. Kim, H. Im, Chemical Engineering Journal, 426 (2021) 130773.

[6] X.F. Lu, S.L. Zhang, W.L. Sim, S. Gao, X.W. Lou, Angewandte Chemie, 133 (2021) 23067-23073.

[7] H. Qin, Y. Ye, J. Li, W. Jia, S. Zheng, X. Cao, G. Lin, L. Jiao, Advanced Functional Materials, 33 (2023) 2209698.

[8.] Coupling regulation for achieving high-efficient UOR performance of amorphous Ni-P catalyst by pulse electrodeposition

[9] Reconstruction of Ni-based catalyst for electrocatalytic urea oxidation reaction

[10] Unprecedented urea oxidation on Zn@Ni-MOF with an ultra-high current density: understanding the competition between UOR and OER, catalytic activity limitation and reaction selectivity

[11]L. Wang, Y. Zhu, Y. Wen, S. Li, C. Cui, F. Ni, Y. Liu, H. Lin, Y. Li, H. Peng, Regulating the local charge distribution of Ni active sites for the urea oxidation reaction, Angew. Chem, 133 (2021) 10671-10676.

[12] X.F. Lu, S.L. Zhang, W.L. Sim, S. Gao, X.W. Lou, Phosphorized CoNi2S4 Yolk-Shell Spheres for Highly Efficient Hydrogen Production via Water and Urea Electrolysis, Angew. Chem, 133 (2021) 23067-23073.

[13] K. Zhang, S. Wang, X. Li, H. Li, Y. Ni, Phase Segregation in Cu0. 5Ni0. 5 Alloy Boosting Urea-Assisted Hydrogen Production in Alkaline Media, Small, (2023) 2300959.

[14] C. Wang, H. Lu, Z. Mao, C. Yan, G. Shen, X. Wang, Bimetal Schottky heterojunction boosting energy-saving hydrogen production from alkaline water via urea electrocatalysis, Adv. Funct. Mater, 30 (2020) 2000556.

[15] X. Gao, X. Bai, P. Wang, Y. Jiao, K. Davey, Y. Zheng, S.-Z. Qiao, Boosting urea electrooxidation on oxyanion-engineered nickel sites via inhibited water oxidation, Nat. Commun, 14 (2023) 5842.

[16] X. Gao, X. Bai, P. Wang, Y. Jiao, K. Davey, Y. Zheng, S.-Z. Qiao, Boosting urea electrooxidation on oxyanion-engineered nickel sites via inhibited water oxidation, Nat. Commun, 14 (2023) 5842.